VOL. 8, NO. 8, AUGUST 2013 ISSN 1819-6608
ARPN Journal of Engineering and Applied Sciences


www.arpnjournals.com

EFFECT OF EXTENDING THE RADIAL SUPERPOSITION FUNCTION TO OTHER FLOW REGIMES

Freddy Humberto Escobar, Hernan Dario Alzate and Leonardo Moreno
Universidad Surcolombiana/CENIGAA, Avenida Pastrana - Cra 1, Neiva, Huila, Colombia
E-Mail: fescobar@usco.edu.co

ABSTRACT

Nowadays, the oil industry is focusing its effort and interest on gas shale reservoirs. Gas shale wells are normally tested by recording the flow rate values under constant pressure conditions. Therefore, time superposition is required in order to conduct transient-rate analysis which normally uses the radial solution of the constant-rate diffusivity equation. This superposition function is also applied indiscriminately to other flow regimes without considering the possibility of an existing error. The literature only reports a case where this situation is dealt with. However, the analysis is performed using curve-decline matching. This study presents the analysis of the effects generated by extending the superposition time function generated with the constant-rate radial solution of the diffusivity equation to other well-known flow regimes. The work consists of performing simulations for the following scenarios: variable rate under constant well-flowing pressure, uncontrolled changes in flow rate, isochronal uncontrolled changes in flow rate, isochronal increasingly changes in flow rate and isochronal decreasingly changes in flow rate. Superposition time functions were generated for each scenario to compare each flow regime (linear, bilinear, elliptical, spherical and pseudo steady state) superposition function to the radial flow superposition function. In general terms, it was found that the generated effects of using the radial time superposition function are negligible. Even, good values of the average reservoir pressure with the radial flow superposition function were obtained. However, it was noted a notorious deviation of the linear and bilinear flow regime tendencies for hydraulically-fractured wells. This leads to erroneous estimation of the fracture parameters.

Keywords: superposition, flow regimes, transient-rate analysis, average reservoir pressure.

1. INTRODUCTION

Pressure drawdown testing (flow tests) has been widely used in the hydrocarbon industry for more than half a century. For such case, the well is set to a constant flow rate. However, in cases which are not possible to keep it constant, a multi-rate test applies and time superposition has to be applied. Multi-rate tests may range from uncontrolled variable rate - Matthews and Russell (1967), Odeh and Jones (1965), series of constant rates - Russell (1963) and Doyle and Sayegh (1970)-, pressure buildup testing and constant bottom-hole pressure with a continuous changing flow rate-Jacob and Lohman (1952). This last technique has been recently named as rate-transient analysis which is very common for testing gas shale formations. In all of them, time superposition has to be applied for the application of the single-rate diffusivity equation solution.

As pointed out by Agnia, Alkouh, and Wattenberger (2012), it has been costumary to use the superposition function obtained from radial flow regime in other flow regimes. Currently, the oil industry is focusing all its efforts on shale reservoirs in which rate-transient analysis is very applied. Therefore, it is important to investigate the impact of the application of the radial superposition function to others flow regimes such as linear and pseudosteady state. Thereby, this study concentrates mainly on the estimating of the superposition time function for linear flow regime and pseudosteady state flow period and estimating the appropriate pressure derivative functions for such cases, so that, comparison with the radial superposition function can be established. Analysis for other flow regimes are also considered. This work complements the investigation recently presented by Agnia *et al*. (2012) with more emphasis in well-test analysis.

Moreover, Escobar, Ibagon and Montealegre-M (2007) presented a metholodogy for estimating the average reservoir pressure from multi-rate tests which is very useful to avoid economical losses due to shutting-in the well. In their development and calculations, they used an arbitrary point on the pseudosteady-state flow period obtained with the equivalent radial superposition time. In this paper, this methodology was also used but changing the the appropriate equivalent pseudosteady state period. Very small differences were found.

2. MATHEMATICAL FORMULATION

Superposition time functions are very useful mathematical tools to handle variable-rate data. The superposition time principle is used to simulate production histories using linear combinations of simple drawdown solutions with different starting times. Assuming no skin effects and only radial flow takes place in the variable rate plot shown in Figure-1, the well pressure at time, t_N, is found by the application of the superposition principle so,

$$P_{wf}(t) = P_i - \frac{141.2\mu B}{kh}\begin{Bmatrix} q_1[P_D(t_D)] + (q_2 - q_1)[P_D([t-t_1]_D)] + \\ (q_3 - q_2)[P_D([t-t_2]_D)] + \\ (q_4 - q_3)[P_D([t-t_3]_D)] \\ +....+(q_N - q_{N-1})[P_D([t-t_N]_D)] \end{Bmatrix} \quad (1)$$

The exponential integral is used in the well-known solution to the single-rate diffusivity equation. It is valid to replace the exponential integral by the natural log

approach after some small flowing times. Then, after some manipulations, Equation (1) becomes (here the skin factor is included),

$$\frac{P_i - P_{wf}(t)}{q_N} = \frac{162.6\mu B}{kh}\left\{\begin{array}{l}\sum_{j=1}^{N}\left(\frac{q_j - q_{j-1}}{q_N}\right)\log\left(t - t_{j-1}\right) + \\ \log\frac{k}{\varphi\mu c_t r_w^2} - 3.2275 + 0.8686s\end{array}\right\} \quad (2)$$

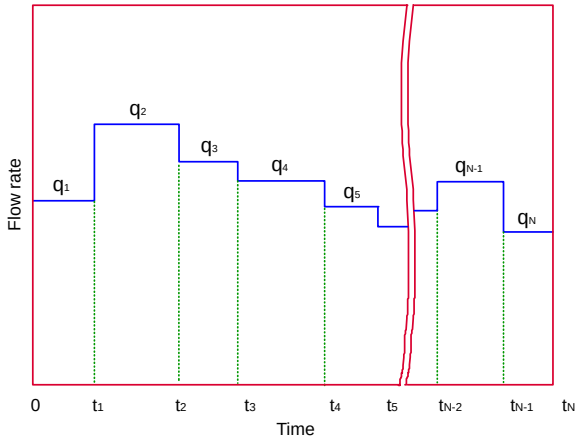

Figure-1. Schematic description of a multi-rate test.

Let,

$$m' = \frac{162.6\mu B}{kh} \quad (3)$$

And,

$$s' = \log\frac{k}{\phi\mu c_t r_w^2} - 3.23 + 0.87s \quad (4)$$

Then, Equation 2 now becomes:

$$\frac{P_i - P_{wf}}{q_n} = m'\sum_{j=1}^{n}\frac{\left(q_j - q_{j-1}\right)}{q_n}\log\left(t - t_{j-1}\right) + b' \quad (5)$$

In which the radial superposition time function is defined as:

$$X_{n\_rad} = \sum_{j=1}^{n}\frac{\left(q_j - q_{j-1}\right)}{q_n}\log\left(t - t_{j-1}\right) \quad (5)$$

And the radial equivalent time is set to be:

$$t_{eq\_rad} = 10^{X_{n\_rad}} \quad (6)$$

In a similar fashion the bilinear, linear, spherical, elliptical and pseudosteady state superposition functions are respectively derived,

$$X_{n\_bil} = \sum_{j=1}^{n}\frac{\left(q_j - q_{j-1}\right)}{q_n}\sqrt[4]{t - t_{j-1}} \quad (7)$$

$$X_{n\_bil} = \sum_{j=1}^{n}\frac{\left(q_j - q_{j-1}\right)}{q_n}\sqrt[4]{t - t_{j-1}} \quad (8)$$

$$X_{n\_lin} = \sum_{j=1}^{n}\frac{\left(q_j - q_{j-1}\right)}{q_n}\sqrt{t - t_{j-1}} \quad (9)$$

$$X_{n\_sph} = \sum_{j=1}^{n}\frac{\left(q_j - q_{j-1}\right)}{q_n}\frac{1}{\sqrt{t - t_{j-1}}} \quad (10)$$

$$X_{n\_ell} = \sum_{j=1}^{n}\frac{\left(q_j - q_{j-1}\right)}{q_n}\left(t - t_{j-1}\right)^{0.36} \quad (11)$$

$$X_{n\_pss} = \sum_{j=1}^{n}\frac{\left(q_j - q_{j-1}\right)}{q_n}\left(t - t_{j-1}\right) \quad (12)$$

With their respective equivalent time functions:

$$t_{eq\_bil} = X_{n\_bil}^4 \quad (13)$$

$$t_{eq\_lin} = X_{n\_lin}^2 \quad (14)$$

$$t_{eq\_sph} = 1/X_{n\_sph}^2 \quad (15)$$

$$t_{eq\_ell} = X_{n\_ell}^{25/9} \quad (16)$$

$$t_{eq\_pss} = X_{n\_pss} \quad (17)$$

In this work, we mainly only concentrated on the radial, linear and pseudo steady state periods. Notice that the treatment for the spherical flow behavior is the same for hemispherical and parabolic flow regimes since the slope in the pressure derivative is negative 0, 5.

3. COMPARISON OF TIME SUPERPOSITION FUNCTIONS

Alzate (2013) perfomed pressure test simulations to observe the above named flow regimes were run with the information provided in Table-1. Table-2 contains the flow rates for the simulation runs. Since the superposition function for radial flow has been extended to other flow regimes, then, it was used as reference point for the comparisons.

The pressure and pressure derivative curve provided in Figure-1 was generated for a constant-flow rate of 300 BPD and information from the second column of Table-1. The analysis was performed first with variable time and uncontrolled variable rate which is referred as

case-1. Then, the rate variation was set isochronally for flow rate changes in an uncontrollable way referred as case-2. Isochronal variations of increasing flow rate changes corresponds to case-3, and the isochronal flow rate decreasing values was called case-4. Also, we extended case-2 for a horizontal well (case-5) and case 2 for a hydraulically-fractured vertical well (case-6). The purpose of these two examples was to compare the radial equivalent time to those of bilinear, elliptical and spherical flow regimes.

Figure-2 shows the normalized pressure derivative for radial, linear and pseudosteady equivalent times. If compared con Figure-1, as expected, the derivative is noisy.

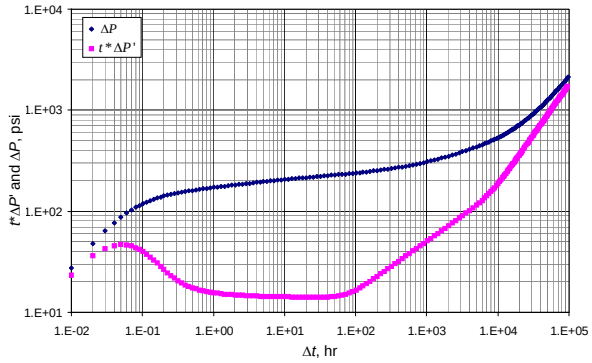

Figure-1. Pressure and pressure derivative log-log plot for a constant production rate case in a rectangular-shaped reservoir.

Table-1. Reservoir and fluid data for example and simulation runs.

Parameter	Cases 1-4	Hydraulic fracture, case-5	Horizontal Well, case-6
P_i, psi	3000	3000	3000
B, bbl/STB	1, 3	1,3	1, 3
h, ft	30	30	100
r_w, ft	0, 3	0,3	0,3
c_t, 1/psi	1, 9x10^{-5}	1,9x10^{-5}	1, 9x10^{-5}
k, md	200	200	43, 42
μ , cp	3	3	3
ϕ , %	0, 1	0,1	0,1
X_E, ft	3000	4000	4000
Y_E, ft	30000	15000	15000
C, bbl/psi	0, 005	0, 005	0, 005
x_f, md		200	
$k_f w_f$, md- ft		5000	
Zw, ft			50
L_w, ft			700

Table-2. Flow rate schedule for uncontrolled changing flow rate.

t, hr	q, BPD
0, 5	300
5, 5	430
64	330
130	380
300	310
800	270
3700	350
4000	425
40000	360
8000	315
20000	225
60000	306

Table-3. Isochronal changing flow rate.

	q, BPD		
t, hr	Uncontrolled changing	Increasing	Decreasing
0,5	209	300	440
3	237	303	418
6	341	318,15	397,1
9	285	321,33	377,25
30	201	337,4	358,39
60	348	340,8	340,46
90	233	357,8	323,44
300	349	361,4	307,27
600	373	379,46	291,9
900	242	383,25	277,31
3000	346	402,41	263,44
6000	339	406,44	250,27
9000	348	426,76	237,76
30000	342	431,03	225,87
60000	307	452,6	214,58
90000	254	457,1	203,85

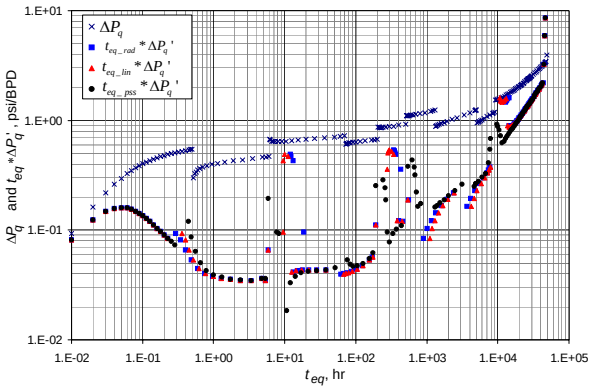

Figure-2. Normalized pressure and normalized pressure derivative log-log plot for radial, linear and equivalent time functions – case-1.

Presents some noise, see Figure-3, the tendency among them is very close. Notice that the noise precedes from two sources: (1) due to the changing rate, and (2) at the end of each flow period, the pressure derivative takes points from other flow regime which increases the noise. Then, in the analysis we will not consider the points close to the time when the flow rate changes.

Since, so far, the radial equivalent time has been used indiscriminately in other flow regime, the idea is to establish a comparison of its failure or acceptance in other flow regimes. Then, the radial equivalent time will be used as comparison point with the equivalent times of the other flow regimes named linear, pseudosteady state, spherical/ hemispherical/parabolic, bilinear and elliptical.

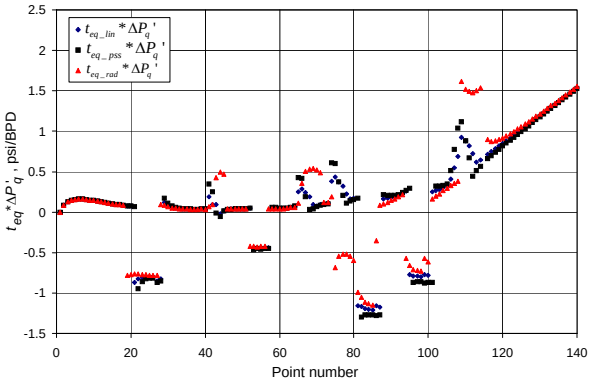

Figure-3. Normalized pressure derivative Cartesian plot for the radial, linear and pseudosteady state equivalent time derivatives – case-1.

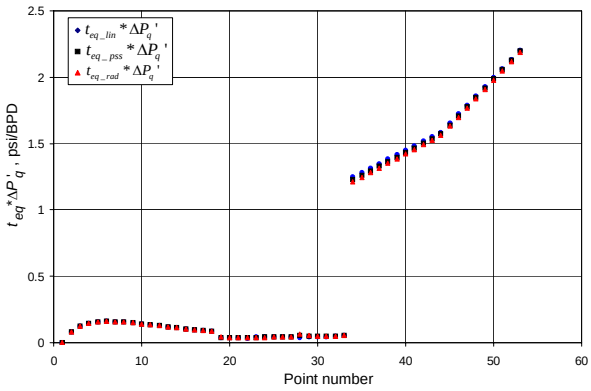

Figure-4. Normalized and filtered pressure derivative **c**artesian plot for the radial, linear and pseudosteady state equivalent time derivatives – case-1.

Notice in Figure-3 how the pressure becomes noisier in the neighborhood of the flow rate changes. Such points were removed and the clean plot was rebuilt in Figure-4. A better definition of the normalized pressure derivative is shown in such plot. Notice that the differences among them are not significant. An Average arithmetic difference between the radial and linear derivatives of 0.0014 psi/BPD was estimated while between the radial and pseudosteady derivatives were 0.0024 psi/STB. Although, the two differences are significantly apart, see Figure-5, we will see later that the effect is negligible in the calculation of the average reservoir pressure.

As indicated before, case-2 deals with isochronal changes in an uncontrollable flow rate. The normalized pressure derivative log-log plot is shown in Figure-6. As expected, the derivative is noisy due to the immoderate changes in flow rate. Figure-6 shows a Cartesian filtered derivative plot in which very small differences among the flow regimes are observed as illustrated in Figure-8. The average differences 0.0099 and 0.017 psi/BPD for radial-linear and radial-pseudosteady state, respectively.

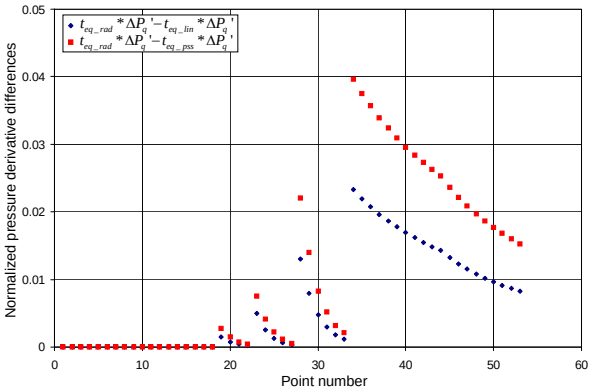

Figure-5. Differences between the radial-linear equivalent normalized derivatives and between the radial-pseudosteady normalized derivatives – case-1.

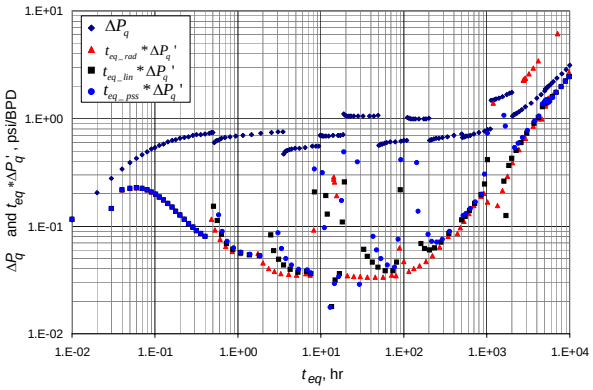

Figure-6. Normalized pressure and normalized pressure derivative log-log plot for radial, linear and equivalent time functions – case-2.

For case-3, the isochronal flow rate change was set increasingly. The normalized pressure derivative curve is presented in Figure-9. Notice that the derivative is smoother than in the former cases due to gradually changes in flow rate. Even though, the filtered derivative values are reported in Figure-10 for comparison purposes and the differences in the derivative values is reported in Figure-11.

The average differences for case-3 are 0.0078 and 0.0011 psi/BPD for radial-linear and radial-pseudosteady state, respectively.

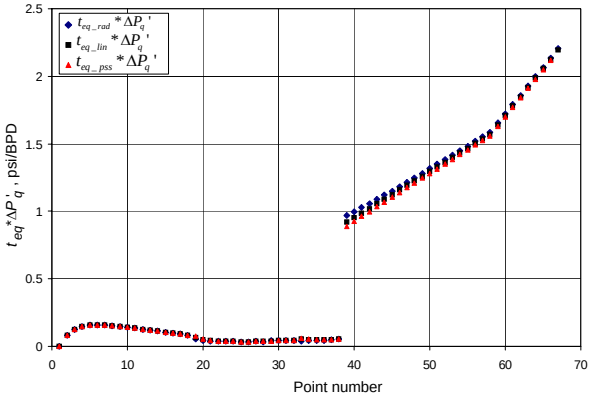

Figure-7. Normalized and filtered pressure derivative **c**artesian plot for the radial, linear and pseudosteady state equivalent time derivatives – case-2.

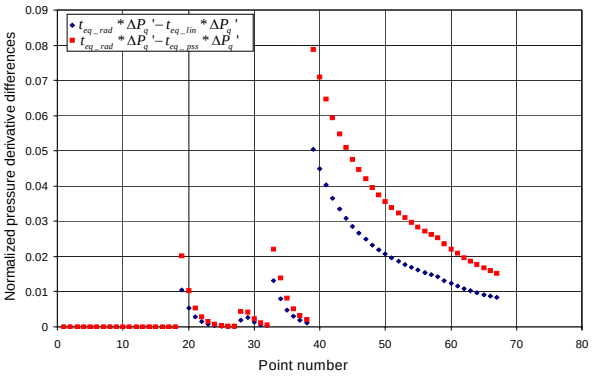

Figure-8. Differences between the radial-linear equivalent normalized derivatives and between the radial-pseudosteady normalized derivatives – case-2.

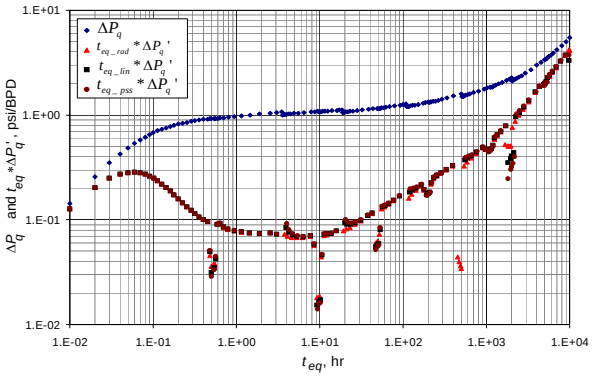

Figure-9. Normalized pressure and normalized pressure derivative log-log plot for radial, linear and equivalent time functions – case-3.

The normalized pressure derivative log-log plot for case-4 - isochronal decreasing flow rate - is shown in Figure-12. Again, the noise is due to the changes in flow rate and the interaction of different flow periods in the estimation of the pressure derivative. As for the former cases a filter was performed and the filtered data are given in Figure-13.

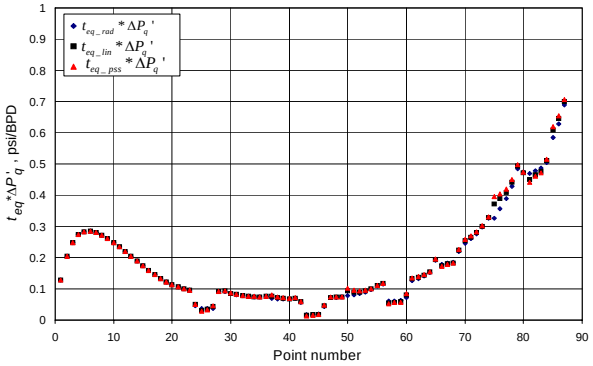

Figure-10. Normalized and filtered pressure derivative **c**artesian plot for the radial, linear and pseudosteady state equivalent time derivatives – case-3.

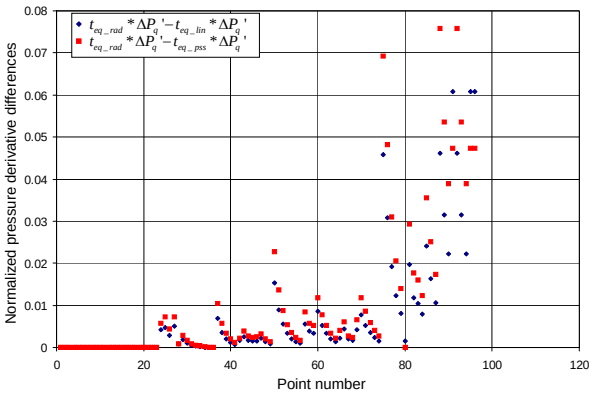

Figure-11. Differences between the radial-linear equivalent normalized derivatives and between the radial-pseudosteady normalized derivatives-case-3.

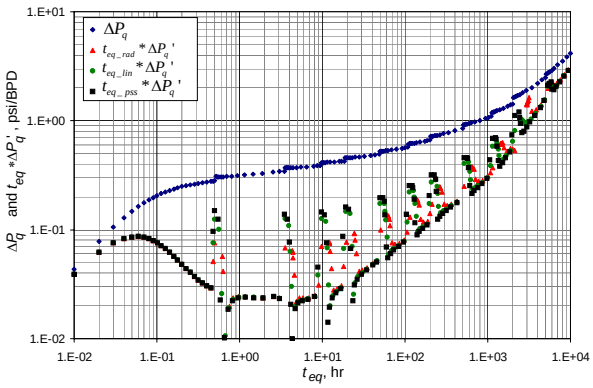

Figure-12. Normalized pressure and normalized pressure derivative log-log plot for radial, linear and equivalent time functions - case 4.

The average differences for case 4 are 0.023 and 0.032 psi/BPD for radial-linear and radial-pseudosteady state, respectively.

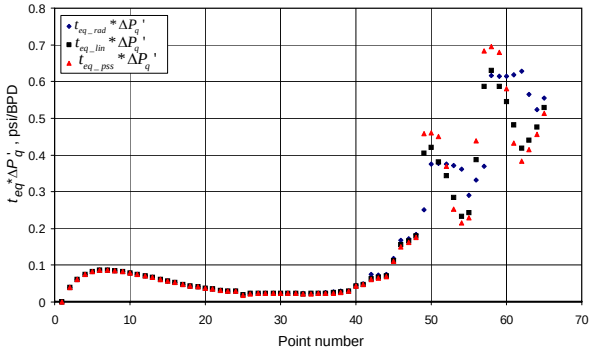

Figure-13. Normalized and filtered pressure derivative **c**artesian plot for the radial, linear and pseudosteady state equivalent time derivatives – case-4.

Case-5 considers a horizontal well in which the elliptical flow regime is observed. For this scenario only the isochronal changes of an uncontrolled flow rate were studied. Figure-15 presents the normalized pressure and pressure derivative log-log plot. Figure-16 is obtained after removing the noisy points due to the change of flow rate. The differences between the radial and elliptical equivalent time derivatives are shown in Figure-17. The average difference between the radial and elliptical normalized derivatives is 0.0043 psi/STB.

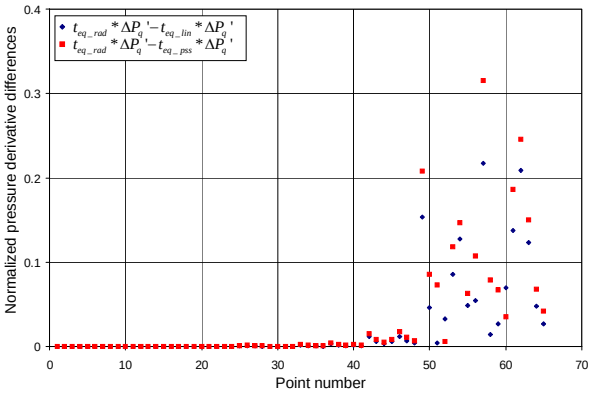

Figure-14. Differences between the radial-linear equivalent normalized derivatives and between the radial-pseudosteady normalized derivatives-case-4.

Case-6 considers a hydraulically-fractured vertical. Both bilinear and parabolic flow regimes are seen. For the parabolic flow the reader is referred to Escobar, Munoz, Sepulveda, and Montealegre (2005). Since the pressure derivative displays a negative one-half slope during the parabolic, hemispherical and spherical flow regimes, in this work, the corresponding time function will be named as if it were the spherical flow. Again, for this situation only the isochronal change of an uncontrolled flow rate was studied.

The average differences for case-6 are 0.0028 and 0.0056 psi/BPD for radial-bilinear and radial-spherical flow regimes, respectively. All the average differences are summarized in Table-4.

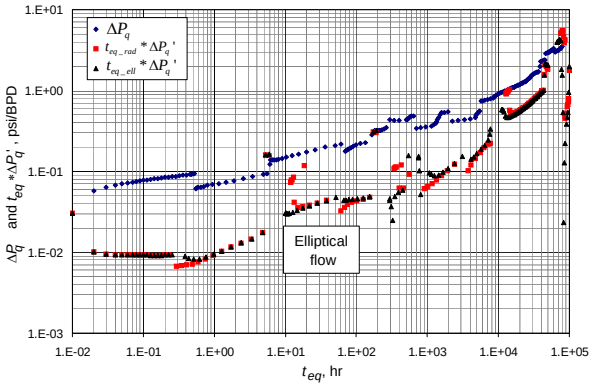

Figure-15. Normalized pressure and normalized pressure derivative log-log plot for radial and elliptical equivalent time functions – case-5.

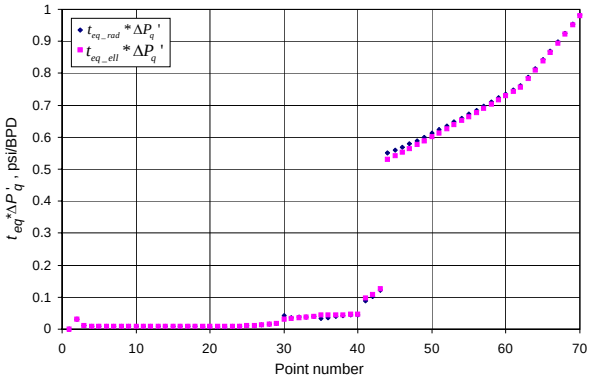

Figure-16. Normalized and filtered pressure derivative **c**artesian plot for the radial and elliptical equivalent time derivatives – case-5.

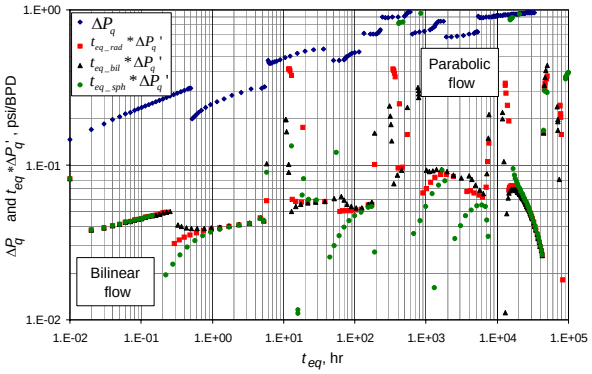

Figure-18. Normalized pressure and normalized pressure derivative log-log plot for radial, bilinear and spherical (parabolic) equivalent time functions – case-6.

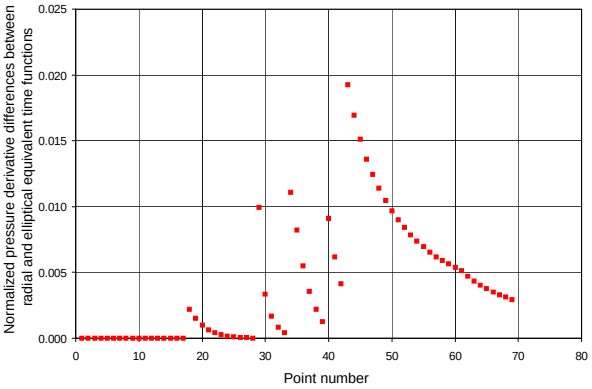

Figure-17. Differences between the radial-elliptical equivalent normalized derivatives- case-5.

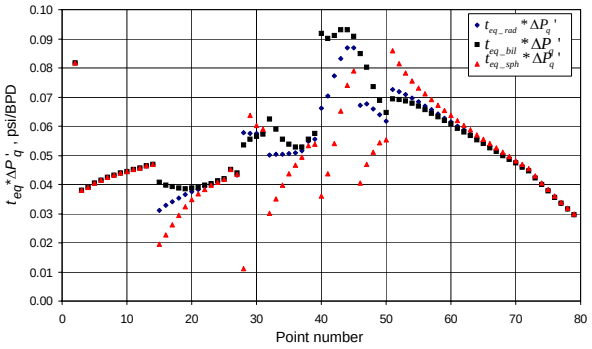

Figure-19. Normalized and filtered pressure derivative Cartesian plot for the radial, bilinear and spherical equivalent time derivatives – case-6.

4. EXAMPLES

Two examples are given to compare the results of an estimation of the average reservoir pressure and the half-length of the fracture, respectively, when the equivalent time functions are appropriately used instead of the radial equivalent time.

Table-4. Summary of average normalized pressure derivative differences.

Case	Radial-linear	Radial -pseudoestable
1	0.00143238	0.00244249
2	0.00999592	0.01701252
3	0.00787595	0.01094802
4	0.02292843	0.03215965
	Radial - bilinear	**Radial-spherical**
5	0.002858	0.00563419
	Radial - elliptical	
6	0.00428172	

4.1. EXAMPLE-1

A multi-rate test was simulated with the information provided in the second column of Table-1. The normalized pressure and pressure derivative log-log plot along with some characteristic points are given in Figure-21. Estimate the average reservoir pressure using the radial equivalent time function and the pseudosteady-state equivalent function.

Solution. Escobar, Ibagon and Montealegre (2007) presented a methodology for the estimation of the average reservoir pressure using the *TDS* technique, Tiab (1993). The shape factor and the average reservoir pressure are estimated using an arbitrary point on the pseudosteady-state period, using the following expressions:

$$C_A = \frac{2.2458A}{r_w^2}\left\{exp\left[\frac{\pi 0.001055kt_{pss}}{\phi\mu c_t A}\left(\frac{(\Delta P_q)_{pss}}{(t*\Delta P_q')_{pss}}-1\right)\right]\right\}^{-1} \quad (18)$$

$$\overline{P} = P_i - \frac{70.6q_n\mu B}{kh}\left[\left(\frac{(t*\Delta P_q')_{pss}}{(\Delta P_q)_{pss}-(t*\Delta P_q')_{pss}}\right)\ln\left(\frac{2.2458A}{C_A r_w^2}\right)\right] \quad (19)$$

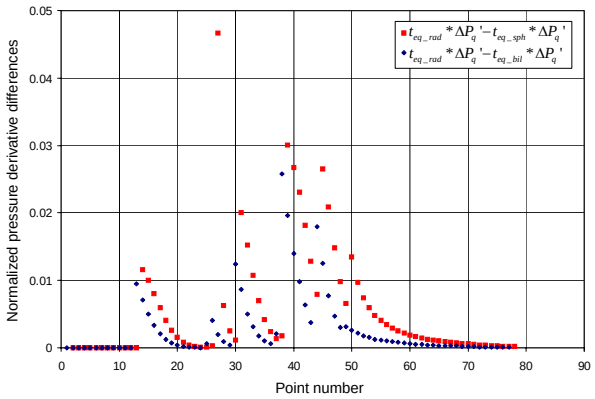

Figure-20. Differences between the radial-spherical equivalent normalized derivatives and between the radial-bilinear normalized derivatives – case-6.

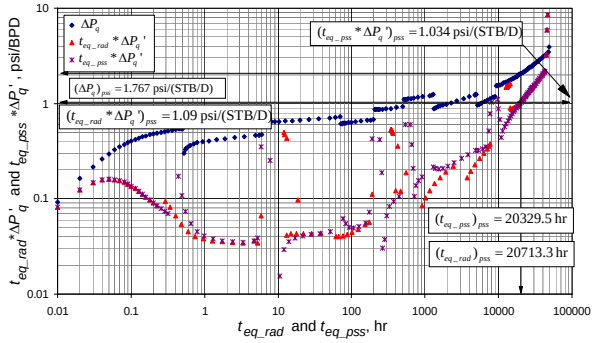

Figure-21. Normalized pressure and normalized pressure derivative log-log plot for example-1.

The following information was read from Figure-21.

$(t_{eq\_rad})_{pss}$ = 20713.3 hr $(t_{eq\_rad}*\Delta P_q')_{pss}$ = 1.09 psi/BPD
$(t_{eq\_pss})_{pss}$ = 20239.5 hr $(t_{eq\_pss}*\Delta P_q')_{pss}$ = 1.034 psi/BPD
$(\Delta P_q)_{pss}$ = 1.767 psi/BPD

The above parameters were used in Equations (1) and (2) to estimate the shape factor and the average reservoir pressure, as reported in Table-4. Although, the shape factors were different, an absolute error of only 0.1 % was found in the estimation of the average reservoir pressure. As noted in Equation (2), the shape factor is inside a natural log which has a small impact in the estimation of the average reservoir pressure.

Table-5. Results for Example-1.

Parameter	Equivalent time function	
	Radial	Pseudosteady
C_A	135.71	18.4
$\bar{P}$	2557.9	2566.1

4.2. EXAMPLE-2

Figure-22 presents synthetic normalized pressure and pressure derivative data for a hydraulically-fractured well. The simulation run was performed using information from the third column of Table-1 for the case of infinite-conductivity fracture. Linear and radial equivalent times are compared in this example. However, the test was also run with a constant flow rate of 300 BPD to observe the deviation of the linear flow as a consequence of the flow rate changes, then, the example will be worked with characteristic derivative points before and after the first flow rate change. The following information was read from Figure-22.

For constant flow rate:

$(t_{eq})_L$ = 0.032 hr
$(t_{eq}*\Delta P_q')_L$ = 0.007 psi/BPD

A slight variation of an expression provided by Tiab, Azzougen, Escobar and Berumen (1999) to estimate the half-fracture length is given as follows:

$$x_f = \frac{2.032B}{h\left(t*\Delta P_q'\right)_L}\sqrt{\frac{\mu t_L}{\phi c_t k}} \qquad (20)$$

A resulting fracture-half length of 199.94 ft was obtained. This agrees very well with the input value of 200 ft.

Reading points before first flow rate change:

$(t_{eq\_rad})_L = (t_{eq\_lin})_L$ = 0.02 hr
$(t_{eq\_rad}*\Delta P_q')_L = (t_{eq\_lin}*\Delta P_q')_L$ = 0.005 psi/BPD

Which gives a half-fracture length of 221.3 ft. When reading the points after first flow rate change:

$(t_{eq\_rad})_L$ = 2.381 hr
$(t_{eq\_lin})_L$ = 2.387 hr
$(t_{eq\_rad}*\Delta P_q')_L$ = 0.020786 psi/BPD
$(t_{eq\_rad}*\Delta P_q')_L$ = 0.020675 psi/BPD

Values of fracture half-length of 583.9 and 581.5 ft were found using radial and linear equivalent time functions, respectively. In both cases the fracture is overestimated more than a 100% since the change of rate deviated the expected tendency of the linear flow regime.

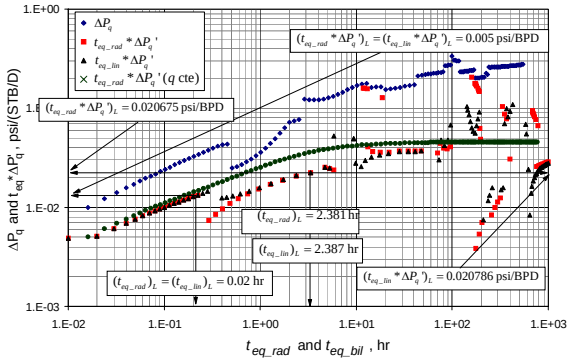

Figure-22. Normalized pressure and normalized pressure derivative log-log plot for example-2.

5. COMMENTS ON THE RESULTS

It can be observed by inspecting the average differences among the normalized functions estimated with the different time functions that the smallest value corresponds to the radial-linear case of increasingly changing rate. However, a general small difference is seen in most of the normalized pressure derivatives. Besides, the plots showing the normalized pressure derivative differences show small differences among all the derivatives with the radial equivalent time function which was selected as reference point since this has been widely used without considering whether or not is valid. The main finding of this work is that the radial equivalent time function can be used in other flow regimes with a neglected difference.

On the other hand, the estimation of the average reservoir pressure provided an absolute deviation error of 0.1% when using the radial and pseudosteady-state time functions which confirms the above statement.

We found, however, that changes in the flow rate deviates the normal behavior of the linear and bilinear flow regimes which leads to erroneous estimation of the fracture parameters.

Decreasing variable rate is recommended to avoid falling below the bubble point pressure.

The finite-difference algorithm for estimation the pressure derivative provides significant noise during the flow rate changes since points on both sides of the flow regime are used, even though, the belong to different tendencies. Then, an improved algorithm is recommended.

6. CONCLUSIONS AND RECOMMENDATIONS

The radial superposition function can be used in other flow regimes with negligible effects.

The estimation of the average reservoir pressure using radial and pseudosteady-state superposition function provided an absolute error 0f 0.1% confirming that the radial superposition function can be used to estimate this parameter. However, the value of the shape factor gave significant differences.

Care should be taken while dealing with hydraulic fractures. The flow rate changes deviate the normal tendency of either the linear and bilinear flow which leads to inaccurate estimation of fracture parameters.

Nomenclature

A	Area, ft^2
B	Volumetric factor, rb/STB
C_A	Dietz shape factor
c_t	System total compressibility, 1/psi
k	Permeability, md
$k_f w_f$	Fracture conductivity, md- ft
L_w	Horizontal well length, ft
P	Pressure, psi
q_n	n-th flow rate , STB/D
t	Time, hr
r	Radius, ft
$t*\Delta P'$	Pressure derivative, psi
$t_{eq}*\Delta P_q'$	Normalized pressure derivative, psi/BPD
ΔP_q	$(P_i - P_{wf})/q_n$
X_E	Reservoir length, ft
x_f	Hydraulic fracture half-length, ft
Y_E	Reservoir width, ft
Z_w	Distance from top to horizontal well, ft

Greeks

Δ	Change, drop
ϕ	Porosity, fraction
μ	Viscosity, cp

Suffices

bil	Bilinear
ell	Elliptical
eq	Equivalent
eq bil	Equivalent bilinear
eq lin	Equivalent linear
eq ell	Equivalent elliptical
eq rad	Equivalent radial
eq pss	Equivalent pseudosteady
eq sph	Equivalent spherical
i	Initial
lin	Linear
L	Linear (any point on linear flow)
r	Radial (any point on radial flow)
rad	Radial
pss	Pseudosteady (any point on pseudosteady state)
sph	Spherical
w	Wellbore

ACKNOWLEDGEMENTS

The authors gratefully thank the Most Holy Trinity and the Virgin Mary mother of God for all the blessing received during their lives.

The authors also wish to thank Mr. Ahmad Alkouh for his help provided by sharing his computer codes for estimating superposition functions.

REFERENCES

Agnia A., Alkouh K. and Wattenberger R.A. 2012. Bias in rate Transient Analysis Methods: Shale Gas Wells. Paper SPE 159710 presented at the SPE ATCE held in San Antonio, TX. October 8-10.

Alzate, H.D. Efectos de Extender Superposición del Flujo Radial a Otros Regimenes de Flujo. Tesis de pregrado. Universidad Surcolombiana. 2013.

Doyle R.E. and Sayegh E.F. 1970. Real Gas Transient Analysis of Three Rate Flow tests. JPT, November. pp. 1347-1356.

Escobar F.H., Munoz O.F., Sepulveda J.A. and Montealegre M. 2005. New Finding on Pressure Response In Long, Narrow Reservoirs. CT and F - Ciencia, Tecnología y Futuro. 2(6): 151-160.

Escobar F.H., Ibagon O.E. and Montealegre-M M. 2007. Average Reservoir Pressure Determination for Homogeneous and Naturally Fractured Formations from Multi-Rate Testing with the *TDS* Technique. Journal of Petroleum Science and Engineering. ISSN 0920-4105. 59: 204-212.

Escobar F.H., Ibagon O.E. and Montealegre-M M. 2007. Average Reservoir Pressure Determination for Homogeneous and Naturally Fractured Formations from Multi-Rate Testing with the TDS Technique. Journal of Petroleum Science and Engineering. 59: 204-212.

Jacob C.E. and Lohman S.W. 1952. Nonsteady Flow to a Well of Constant Drawdown in an Extensive Aquifer. Trans., AGU, August. pp. 559-569.

Matthews C.S. and Russell D. G. 1967. Pressure Buildup and Flow Tests in wells. Monograph series. Society of Petroleum Engineers of AIME, Dallas, TX. 1, chap. 6.

Odeh A.S. and Jones L.G. 1965. Pressure Drawdown Analysis, Variable Rate Case. JPT, August. Trans. AIME 234. pp. 960-964.

Russell D.G. 1963. Determination of Formation Characteristics from Two-Rate Flow Tests. JPT, December. Trans. AIME 228. pp. 1347-1355.

Tiab D. 1993. Analysis of Pressure and Pressure Derivative without Type-Curve Matching: 1- Skin and Wellbore Storage. Journal of Petroleum Science and Engineering. 12: 171-181.

Tiab D., Azzougen A., Escobar F. H. and Berumen S. 1999. Analysis of Pressure Derivative Data of a Finite-Conductivity Fracture by the Direct Synthesis Technique. Paper SPE 52201 presented at the 1999 SPE Mid-Continent Operations Symposium held in Oklahoma City, OK, March 28-31.